1

2

3 **Main Manuscript for**

4 Wetting of phase-separated droplets on plant vacuole membranes 5 leads to a competition between tonoplast budding and nanotube 6 formation

7

8 Halim Kusumaatmaja[1]*, Alexander I. May[2,3#], Mistianne Feeney[4,5#], Joseph F. McKenna[4], Noboru
9 Mizushima[6], Lorenzo Frigerio[4]* and Roland L. Knorr[6]*

10

11 [1] Dept. of Physics, University of Durham, Durham, United Kingdom
12 [2] Tokyo Tech World Research Hub Initiative, Institute of Innovative Research, Tokyo Institute of
13 Technology, Kanagawa, Japan
14 [3] Cell Biology Center, Institute of Innovative Research, Tokyo Institute of Technology, Yokohama,
15 Japan
16 [4] School of Life Sciences, University of Warwick, Coventry, UK
17 [5] Tropic Biosciences UK LTD, Norwich, UK
18 [6] Graduate School and Faculty of Medicine, The University of Tokyo, Tokyo, Japan

19

20 [#] Equal contribution

21

22 * Halim Kusumaatmaja, Lorenzo Frigerio, Roland L. Knorr
23 **Emails:** halim.kusumaatmaja@durham.ac.uk, L.Frigerio@warwick.ac.uk, knorr@m.u-tokyo.ac.jp

24

25 **Author Contributions:** R.L.K., H.K., and L.F. conceived the project. H.K. developed the theory.
26 R.L.K., M.F., J.F.M. supported by L.F. and N.M. performed the experiments and analysed data.
27 R.L.K., H.K., and A.I.M. and wrote the manuscript. All authors discussed the results and
28 commented on the manuscript.

29

30 **Competing Interest Statement:** The authors declare no competing conflicts of interest.

31

32 **Classification:**
33 PHYSICAL SCIENCES/ Biophysics and Computational Biology
34 BIOLOGICAL SCIENCES/ Plant Biology

35

36 **Keywords:** Protein storage vacuole, membrane remodeling, wetting, phase separation, plant
37 development

38

39 **This file includes:**
40 Main Text
41 Figures

42

43 **Abstract**
44 Seeds of dicotyledonous plants store proteins in dedicated membrane-bounded organelles called
45 protein storage vacuoles (PSVs). Formed during seed development through morphological and
46 functional reconfiguration of lytic vacuoles in embryos (Feeney et al. Plant Phys. 2018) (1), PSVs
47 undergo division during the later stages of seed maturation. Here, we study the biophysical
48 mechanism of PSV morphogenesis in vivo, discovering that micrometer-sized liquid droplets
49 containing storage proteins form within the vacuolar lumen through phase separation and wet the
50 tonoplast (vacuolar membrane). We identify distinct tonoplast shapes that arise in response to
51 membrane wetting by droplets and derive a simple theoretical model that conceptualizes these
52 geometries. Conditions of low membrane spontaneous curvature and moderate contact angle
53 (i.e. wettability) favor droplet-induced membrane budding, thereby likely serving to generate
54 multiple, physically separated PSVs in seeds. In contrast, high membrane spontaneous curvature
55 and strong wettability promote an intricate and previously unreported membrane nanotube
56 network that forms at the droplet interface, allowing molecule exchange between droplets and the
57 vacuolar interior. Furthermore, our model predicts that with decreasing wettability, this novel
58 nanotube structure transitions to a regime with bud and nanotube coexistence, which we
59 confirmed in vitro. As such, we identify intracellular wetting (Agudo-Canalejo et al. Nature 2021)
60 (2) as the mechanism underlying PSV morphogenesis and provide evidence suggesting that
61 interconvertible membrane wetting morphologies play a role in the organization of liquid phases in
62 cells.
63
64 **Results and Discussion**
65 A hallmark of seed maturation in plant embryos is the remodeling and division of preexisting
66 single vacuoles into multiple PSVs as these organelles accumulate storage proteins (1). The
67 mechanism that drives this transition is unclear. To better understand the process of PSV
68 morphogenesis, we performed live-cell imaging of fluorescently labeled tonoplasts in embryos of
69 the plant model *Arabidopsis thaliana* under previously reported conditions (1), observing single
70 large vacuoles containing a homogeneous luminal solution at an early developmental stage (Fig.
71 1A-C). We also observed vacuoles containing curved and dynamic membrane structures that
72 derive from the tonoplast and have a diameter below the optical resolution limit (Fig. 1C, Movies
73 S1,2). We name these structures nanotubes to distinguish them from trans-vacuolar strands,
74 straight tubules with a diameter of 1-3 µm (3). At developmentally later stages, we detected the
75 occurrence of large vacuolar sub-compartments: luminal droplets that accumulate the storage
76 protein 2S1-GFP and are stained by neutral red (1). Contact between such droplets and the
77 tonoplast invariably results in deformation of droplets into spherical cap shapes, indicative of
78 droplets that wet surfaces. Subsequently, storage protein droplets deform contacting tonoplasts,
79 generating tonoplast ridges and subsequently buds that apparently enclose droplets (Fig. 1D).
80 These findings are similar to polymer droplets that form by liquid-liquid phase separation and
81 subsequently wet and deform membranes to induce bud formation in vitro (4, 5).
82 We next sought to determine the physical nature of vacuolar droplets. Time-lapse
83 imaging showed their spontaneous formation by a phase separation-like process, with droplet
84 flow, droplet fusion and droplet repositioning all observed, providing evidence for liquid-like
85 droplet properties (Fig. 1G, H; Movies S3, S4). Fluorescence recovery after photobleaching
86 (FRAP) analysis of 2S1-GFP demonstrated rapid recovery with a half time of 2.4±1.2 s and a
87 large mobile fraction of 70.1±5.5% (Fig. 1I). Addition of hexanediol dissolved droplets (Movie S5)
88 and, concomitant with droplet dissolution, tonoplast ridges previously associated with contact
89 lines disappeared (Movie S6). Droplets reformed, again exhibiting droplet fusion and tonoplast
90 wetting events upon hexanediol washout (Movie S7). Moreover, all tonoplast-derived nanotubes
91 appeared to maintain contact with droplet interfaces (Fig. 1E, F). Together, these findings
92 strongly indicate that vacuolar droplets are phase-separated liquids that wet and deform
93 tonoplasts and tonoplast-derived nanotubes.
94 To physically describe droplet-mediated organelle remodeling, we developed a
95 theoretical model that explains the interplay between tonoplasts and two liquid compartments, α
96 and β. Tonoplast membranes form nanotubes (Fig. 1C) that are recruited to the droplet interface

97 $\alpha\beta$ (Figs. 1E, F, 2A) and have a diameter below the optical resolution limit (< 0.2 μm). We
98 exploited the length difference between nanotubes and tonoplasts (~10 μm) to calculate the
99 energy contributions of membrane spherical caps, E_{cap}, and membrane nanotubes, E_{tube}. To
100 compute E_{cap}, we assume that contributions from interfacial terms dominate bending terms. For
101 E_{tube}, we account for the interfacial energy and bending of cylindrical nanotubes while assuming
102 they are immersed at the droplet interface, $\alpha\beta$, with an angle equal to the intrinsic contact angle,
103 θ_{in} (Fig. 2A, Extended Theoretical Methods). Such adsorption lowers the interfacial energy. The
104 contact angle θ_{in} quantifies the relative interaction strength between α, β and the membrane.
105 By minimizing the total energy of the system $E_{\text{total}} = E_{\text{cap}} + E_{tube}$, we identified three
106 distinct morphological regimes depending on two key parameters: the contact angle θ_{in} and the
107 normalized spontaneous curvature $\widetilde{m} = \left(8\kappa m^2/\Sigma_{\alpha\beta}\right)^{1/2}$ (Fig. 2B). Here, m is the membrane
108 spontaneous curvature, κ is the membrane bending rigidity and $\Sigma_{\alpha\beta}$ denotes the droplet
109 interfacial energy. In regime I, small $\widetilde{m}$ values do not favor the formation of membrane
110 nanotubules; instead, excess membrane area results in budding only. For larger $\widetilde{m}$, nanotubes
111 form and localize to $\alpha\beta$ in two distinct morphologies: either coexisting with membrane buds
112 (regime II, intermediate $\widetilde{m}$) or forming as a network of nanotubes exclusively, without buds
113 (regime III, high $\widetilde{m}$). We found that as θ_{in} increases, all regime boundaries shift to higher $\widetilde{m}$
114 values (Fig. 2B). We identified the boundary between regimes I and II to be when the nanotube
115 area, A_{tube}, deviates from zero. To distinguish regimes II and III, we employed a criterion based
116 on the apparent reduced organellar volume being close to a spherical shape with $v_a =$
117 $(V_{\text{total}})/\left[(4\pi/3) \times (A_{\text{c}}/4\pi)^{3/2}\right] = 0.99$, with A_c corresponding to the membrane area stored in both
118 spherical caps and V_{total} accounting for volumes of both interior liquids α and β. The
119 phenomenon observed is robust: variations in v_a only slightly shift the regime boundary. Hence,
120 droplet-mediated organelle remodeling can be understood as a competition between nanotube
121 and bud formation.
122 Consistent with our model, we observed three tonoplast morphologies in living embryos
123 (Fig. 1D-F). However, whether and how droplet and membrane physical parameters change to
124 affect tonoplast shape transformations is not known. While regimes I and II have previously been
125 observed in vitro using vacuole-sized vesicles enclosing two polymer liquids (6, 7 and Extended
126 Experimental Methods), regime III has not. In this experimental system, increased osmotic
127 pressure raises both $\Sigma_{\alpha\beta}$ and θ_{in} (8). In agreement with our model, we observed regime III
128 shapes that were stable for over 10 hours under conditions of low osmotic pressure close to the
129 polymer phase separation point (i.e. characterized by low $\Sigma_{\alpha\beta}$ and θ_{in}; Fig. 2C). Meanwhile,
130 under high osmotic pressure we observed regime II shapes (Fig. 2D). Using time-lapse imaging,
131 we directly confirmed that exposure of regime III vesicles to hyperosmotic stress induced regime
132 III to II remodeling (Fig. 2E), as predicted by our model.
133 Our models rationalize tonoplast remodeling, a main morphological event during PSV
134 formation, using simple theoretical and in vitro parameters. While our models recapitulate key
135 PSV shapes, how PSVs form is still not well characterized and future investigations must address
136 differences between in vivo PSVs and modeled predictions for controlled conditions. For
137 example, we observed that single preexisting vacuoles generate many PSVs, and that tonoplasts
138 are not immediately deformed by storage protein droplets. Multiple PSVs might result from
139 tonoplast ridges that form between adjacent droplets, thereby limiting droplet fusion and causing
140 consecutive rounds of droplet formation and budding. Further, the combination of ongoing
141 storage protein accumulation, water efflux and decreasing pH likely provides a means of tuning
142 droplet properties, tonoplast charge and membrane spontaneous curvatures, thereby controlling
143 organellar wetting morphologies. In addition, external factors such as tonoplast-cytoskeleton
144 linkages, the viscoelasticity of the cytosol, and a broad range of organelles including oil bodies
145 might slow and sterically constrain tonoplast deformation substantially, while low droplet
146 interfacial tension and an absence of membrane excess area might prevent membrane
147 deformation altogether. Indeed, the process of Arabidopsis PSV formation is known to be
148 asynchronous and slow, taking several days (1).

Beyond understanding the functional basis of protein accumulation for crop improvement, our findings promise a means of engineering PSVs, potentially allowing for the development of new sources of high-value proteins (9). We show that together, droplet and membrane material properties determine whether networks of nanotubes wet droplets or droplet-mediated membrane buds form. Our data suggest that budding is the mode of PSV formation with functional implications for their development: while a bud can reversibly separate two liquid phases and establish distinct intracellular milieus by enclosing each within physically discrete membranes, wetting nanotube networks provide a structure allowing for molecule exchange between both liquid phases (Fig. 2B, C). This work demonstrates both how droplets provide a liquid structure for assembling competing membrane shapes, as well as a novel example of how membrane wetting organizes liquids in cells.

Materials and Methods

All data, materials and equations needed to evaluate the conclusions in the paper are provided in the paper. Additional data related to this manuscript may be requested from the authors.

Acknowledgments

We thank Kengo Watanabe and Hidenori Ichijo (Graduate School of Pharmaceutical Sciences, UT) for providing access to the osmometer. R.L.K. and H.K. thank colleagues at MPI-CI for discussion. R.L.K. thanks the Warwick Institute for Advanced Studies for an International Visiting Fellowship, Chieko Saito for inspiration (UT), Christian Schmitz-Linneweber and Thomas Korte (HU Berlin) for support. N.M. was supported by the Exploratory Research for Advanced Technology via the Japan Science and Technology Agency (JPMJER1702). LF and JMcK were supported by a grant from the Leverhulme Trust (RPG-20-013). AIM was supported by JSPS KAKENHI Grant Number JP21K15083.

References

1. M. Feeney, M. Kittelmann, R. Menassa, C. Hawes, L. Frigerio, Protein storage vacuoles originate from remodelled pre-existing vacuoles in Arabidopsis thaliana. *Plant Physiology* **177**, 241–254 (2018).

2. J. Agudo-Canalejo, *et al.*, Wetting regulates autophagy of phase-separated compartments and the cytosol. *Nature* **591**, 142–146 (2021).

3. D. Reisen, F. Marty, N. Leborgne-Castel, New insights into the tonoplast architecture of plant vacuoles and vacuolar dynamics during osmotic stress. *BMC Plant Biology* **5**, 13 (2005).

4. H. Kusumaatmaja, Y. Li, R. Dimova, R. Lipowsky, Intrinsic Contact Angle of Aqueous Phases at Membranes and Vesicles. *Phys. Rev. Lett.* **103**, 238103 (2009).

5. S. Botterbusch, T. Baumgart, Interactions between Phase-Separated Liquids and Membrane Surfaces. *Applied Sciences* **11**, 1288 (2021).

6. L. M. Dominak, E. L. Gundermann, C. D. Keating, Microcompartmentation in Artificial Cells: pH-Induced Conformational Changes Alter Protein Localization. *Langmuir* **26**, 5697–5705 (2010).

7. Y. Li, R. Lipowsky, R. Dimova, Membrane nanotubes induced by aqueous phase separation and stabilized by spontaneous curvature. *PNAS* **108**, 4731–4736 (2011).

8. Y. Liu, J. Agudo-Canalejo, A. Grafmüller, R. Dimova, R. Lipowsky, Patterns of Flexible Nanotubes Formed by Liquid-Ordered and Liquid-Disordered Membranes. *ACS Nano* **10**, 463–474 (2016).

195 196 9. J. Schwestka, *et al.*, Plant-derived protein bodies as delivery vehicles for recombinant proteins into mammalian cells. *Biotechnol Bioeng* **117**, 1037–1047 (2020).

197
198

199 **Figures**
200
201 **Figure 1. Liquid droplets wet and deform vacuolar membranes in living plant embryos.**
202 (A) *A. thaliana* embryo at walking stick developmental stage. (B) Embryonic cotyledon (leaf)
203 expressing the tonoplast protein GFP-TPK1 (membrane, green). (C) Homogeneous vacuolar
204 lumina characteristic of young vacuoles. Arrowheads, tonoplast-derived nanotubes. Individual
205 frame from Movie S1. (D) Vacuolar liquid sub-compartments α and β wet enclosing tonoplast.
206 The droplet interface $\alpha\beta$ causes vacuole deformation and budding. (E, F) Tonoplast nanotubes
207 wet the droplet interface. (G, H) Spontaneous droplet formation, flow, fusion and repositioning
208 observed by live-cell imaging. Snapshots from data shown in movies S3, 4. (I) Individual droplet
209 FRAP data (blue dots). Fitted curves, black lines, *n* = 14 across three independent experiments.
210 Red line, global fit. Inset, representative time series. Mean ± SD. Confocal live cell imaging.
211 Vacuolar lumina (magenta) stained by 20 µM neutral red (NR) or expression of 2S1-GFP. Scale
212 bars, 2.5 µm (white), 100 µm (black).
213
214 **Figure 2. Theoretically predicted and experimentally observed droplet-membrane wetting**
215 **morphologies.** (A) Contact line geometry for membrane nanotubes and buds. (B) The
216 morphology diagram predicts three distinct wetting regimes as sketched. (C-E) In vitro validation
217 of model predictions using vacuole-sized vesicles (green) enclosing polymer liquids α (unlabeled)
218 and β (magenta). (C) Low θ_{in} and interfacial tension produce regime III. Left, confocal section
219 orthogonal to center and right panels, as indicated. (D) High θ_{in} and interfacial tension generate
220 regime II. (E) Time series of a transition from regime III to II obtained by hyperosmotic stress,
221 increasing θ_{in} and interfacial tension. Arrowheads, visible nanotube network. Confocal
222 microscopy. Rotational symmetry axes are indicated. Scale bars, 5 µm.

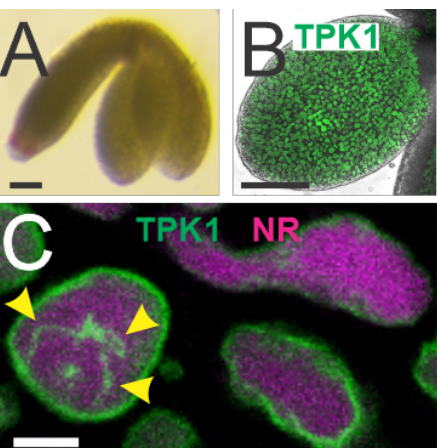
A
B
TPK1
C
TPK1
NR

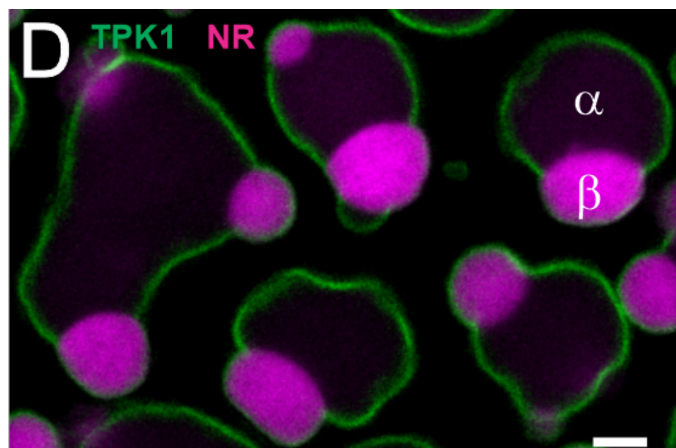
D
TPK1
NR
α
β

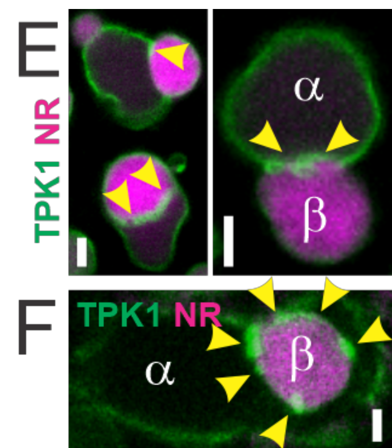
E
TPK1 NR
α
β
F
TPK1 NR
α
β

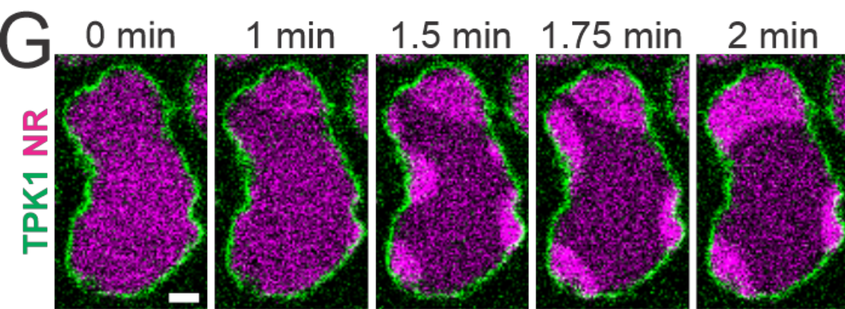
G
0 min
1 min
1.5 min
1.75 min
2 min
TPK1 NR

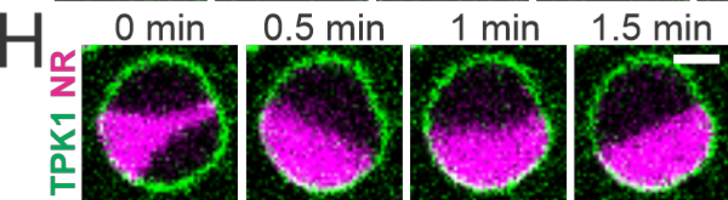
H
0 min
0.5 min
1 min
1.5 min
TPK1 NR

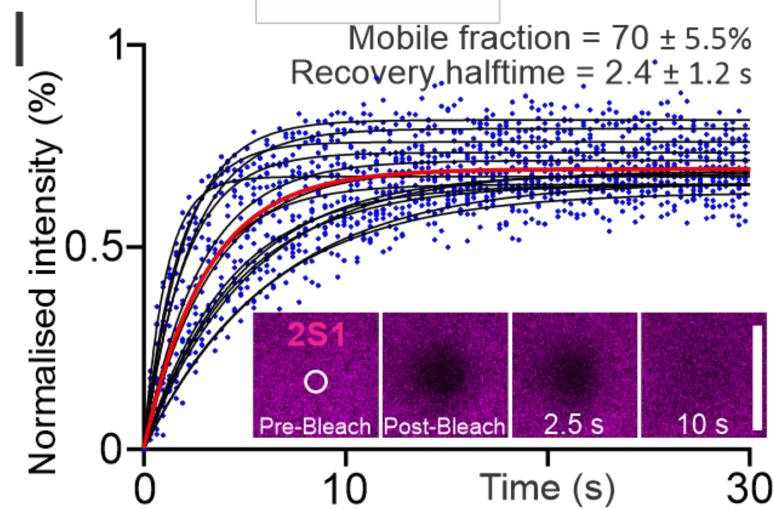
I
Mobile fraction = 70 ± 5.5%
Recovery halftime = 2.4 ± 1.2 s
Normalised intensity (%)
1
0.5
0
0
10
Time (s)
30
2S1
Pre-Bleach
Post-Bleach
2.5 s
10 s

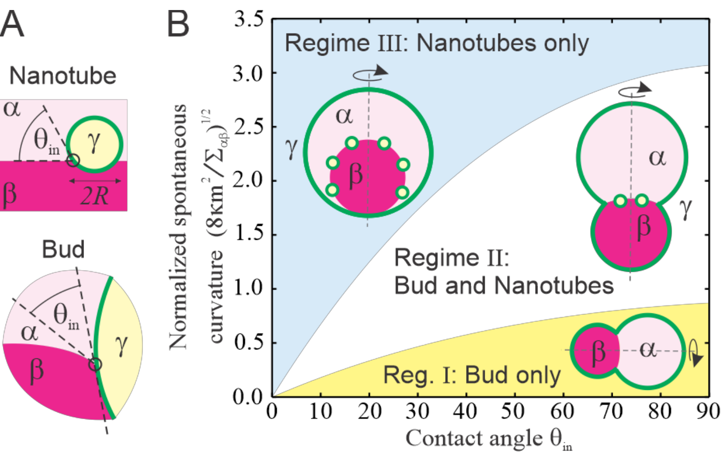
A
Nanotube
α
θ_{in}
γ
β
2R
Bud
α
θ_{in}
β
γ
B
Regime III: Nanotubes only
Regime II:
Bud and Nanotubes
Reg. I: Bud only
Normalized spontaneous curvature $(8\kappa m^2/\Sigma_{\alpha\beta})^{1/2}$
Contact angle θ_{in}

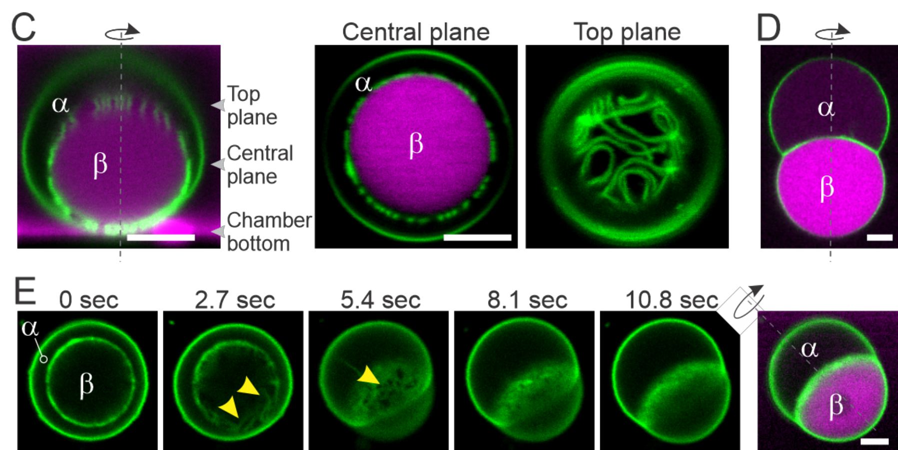
C
Top plane
Central plane
Chamber bottom
Central plane
Top plane
D
E
0 sec
2.7 sec
5.4 sec
8.1 sec
10.8 sec